

THRESHOLD STRESS MEASUREMENTS IN SHOCK-DEFORMED COPPER

Paul S. Follansbee and George T. Gray
Los Alamos National Laboratory
Los Alamos, N.M.

INTRODUCTION

Shock recovery experiments provide a useful technique to investigate the response of materials to extreme conditions of strain rate, imposed hydrostatic pressure, and temperature. Many previous investigators of deformation mechanisms during the passage of shock waves have chosen pure FCC metals (such as Cu and Ni) for study since these metals do not undergo solid-state phase transitions and since the quasi-static mechanical properties and microstructural deformation mechanisms of these metals are generally well understood. Significant findings of some of these earlier investigations have been reviewed by Leslie¹, Murr², and Mikkola and Wright³. It has been well documented for FCC metals that shock wave deformation leads to higher hardness values, dislocation densities⁴, stored energies⁵ and residual stresses⁶ than quasi-static deformation to the same "equivalent" strain.

In FCC metals that form distinct cell structures, the cell size resulting from shock-deformation is typically less than that formed quasi-statically². One important difference noted between microstructures formed by shock-deformation and those formed by quasi-static deformation is the increased contribution of deformation twinning in the latter^{1,3}. The extent of deformation twinning increases with increasing shock pressure. Another microstructural difference between quasi-static and shock-deformation is the observed increase in the levels of vacancy generation in shock-deformation; evidence for this has been reviewed by Graham⁷.

Summarizing these previous studies of the shock-deformation behavior of Cu and Ni, one would conclude that at moderate shock pressures the deformation mechanisms involve dislocation multiplication and dislocation/dislocation interactions similar to those processes that have been documented at quasi-static strain rates. As the shock pressure, and thus the imposed strain rate, is increased deformation twinning becomes increasingly important. The influence of the observed increased levels of vacancy production on deformation mechanisms remains an open question.

In FCC metals the resistance that a dislocation experiences as it moves along a glide plane is illustrated in Fig. 1.⁸ This figure shows schematically two obstacles separated by a distance λ_2 . These obstacles could be forest dislocations, solute atoms or even vacancy clusters. The obstacle height is the mechanical threshold $\hat{\sigma}$, which represents the stress that must be applied in the absence of thermal activation to push a

dislocation past the obstacle. At quasi-static strain rates thermal activation assists the applied stress and allows dislocation motion at stresses below $\hat{\tau}$. Under dynamic conditions the applied stress may actually exceed $\hat{\tau}$; in this case, the velocity of the dislocation as it moves the distance λ_2 between obstacles becomes rate controlling. One important consequence of the glide resistance profile for FCC metals shown in Fig. 1 is that during transit between obstacles the stress driving the dislocation velocity is essentially the applied stress. In other crystal structures, a lattice friction or Peirel's stress component may oppose the applied stress.

The height and shape of the obstacle profile for the dominant obstacle provide information on the nature of the deformed microstructure. These quantities can be measured on recovered shock-deformed material using the technique outlined previously^{9,10}. The purpose of this paper is to further investigate shock wave deformation mechanisms by measuring the mechanical threshold, or threshold stress, on shock deformed material. Oxygen-free-electronic (OFE) copper was selected for this study since its shock-deformation behavior has been extensively studied and since these shock-deformation results complement extensive measurements¹⁰ at strain rates up to 10^4 s^{-1} . Measurements of the mechanical threshold, their implications regarding deformation mechanisms and correlation with the microstructure characterized with TEM are described in this paper.

EXPERIMENTAL

The OFE Cu was obtained in the form of 12.7 mm thick plate. Specimens for the shock recovery experiment, to be detailed below, were machined from this starting material and annealed at 600 C in vacuum for one hour to yield the desired recrystallized grain structure with equiaxed grains of 40 μm average dimension.

The shock recovery experiments were performed utilizing a 40 mm single-stage gas gun. The specimen configuration used consisted of a 4.76 mm thick, 12 mm diameter tapered (10°) sample tightly fitting into two concentric copper momentum trap rings with outside diameters of 25 mm and 42 mm (Fig. 2). The sample surface was protected from impact and the entire sample from spallation by a close-fitting copper cover plate (2.5 mm thick) and spall plate (12 mm thick), respectively. All specimen assembly components were machined to a #32 or better finish and separated by a thin layer of vacuum grease to eliminate "hot spots" during the shock-loading process. The taper, concentric momentum rings, and component surface finish have been found by previous design testing to minimize converging release wave effects resulting in nearly pure uniaxial loading and release with little residual sample strain.

The copper sample was shocked to 10 GPa for 1 μs pulse duration by impacting a 2.26 mm thick copper flyer plate, fixed to a low-impedance aluminum honeycomb-filled projectile, at 518 m/s with the specimen assembly in a vacuum ($< 2 \text{ Pa}$). This shock pressure for copper translates

into a transient strain of 0.0825 using the relation $\epsilon_s = 4/3 \ln(V/V_0)$. Following the removal of the shock-loaded specimen from a water-recovery tank, four compression specimens were electron-discharge machined (EDM) from the recovered disc. Thickness measurements following shock-loading revealed a final sample thickness varying over the sample between 4.63 mm and 4.70 mm compared to a pre-shot thickness of 4.72 mm. The compression specimens averaged 4.5 mm in length by 4.3 mm in diameter. It should be emphasized that for these experiments no precautions were taken to minimize recovery processes in the time period between the shock-deformation and the quasi-static reloading.

The reloading operation was performed at a strain rate of 0.0015 s^{-1} with a screw-driven mechanical testing machine equipped with a specially designed subpress which could be completely immersed in liquid nitrogen. Two specimens were reloaded at room temperature (297 K) while the remaining two were reloaded at liquid nitrogen temperature (76 K).

Samples for optical metallography and transmission electron microscopy (TEM) were sectioned from the pieces of the shock-deformed disc which remained after the compression specimens were removed. Wafers for TEM examination were initially chemically thinned to 0.13 mm in a solution of 50% H_3PO_4 , 40% HNO_3 and 10% HCl at 25 C. Discs 3 mm in diameter were then punched and electropolished in a solution of 25% H_3PO_4 and 75% H_2O at 0 C utilizing a current density of 80 mA/mm^2 . Observation of the foils was made using a Phillips 400 at 120 KV utilizing a goniometer-tilt stage.

RESULTS

Mechanical Threshold Measurements

The four stress strain curves for the reloads at 297 K and 76 K are shown in Fig. 3. There is a hint of a yield drop for the 297 K curves, which is not evident in the 76 K curves. These results are similar to those reported by Appleton and Waddington using tensile reloads¹¹. The yield points, determined by back-extrapolating the work hardening behavior at strains to $\epsilon = 0.10$, for the 297 K curves are 245 MPa and 249 MPa while those for the 76 K curves are 307 MPa and 313 MPa.

The mechanical threshold is the yield stress at 0 K, which we determine by extrapolation. The extrapolation procedure, which has been described previously^{9,10}, is outlined below. For the quasi-static strain rate of the reload experiments, the deformation is thermally activated and can be represented by an equation of the form

$$\dot{\epsilon} = \dot{\epsilon}_0 \exp - \frac{\Delta G}{kT} , \quad (1)$$

where $\dot{\epsilon}_0 = \frac{\rho_m b \lambda^2}{M \nu_0^{-1}}$ (2)

and ΔG is the activation energy. In Eq. 2, ρ_m is the mobile dislocation density, b is the Burgers vector, M is the Taylor factor, and ν_0 is the attempt frequency. When short range obstacles are rate controlling, the activation energy can be approximated by⁸

$$\Delta G = \mu b^3 g_0 \left\{ 1 - \left(\frac{\sigma}{\sigma_0} \right)^{1/2} \right\}^{1/2} , \quad (3)$$

where g_0 is the normalized activation energy. The exponents 1/2 and 3/2 in Eq. 3 are chosen to represent the obstacle profile for short range obstacles⁸.

Extrapolation to 0 K requires that the temperature dependence of the activation energy ΔG be added to the intrinsic temperature dependence (kT) given by Eq. 3. Assuming that the temperature dependence of the activation energy is equal to that of the shear modulus μ , $\Delta G(T) = \mu(T)b^3g_0$, then the extrapolation to 0 K is given by combining and rearranging Eqs. 3 and 1 to give

$$\left(\frac{\sigma}{\mu(T)}\right)^{1/2} = \left(\frac{\hat{\tau}}{\mu(T)}\right)^{1/2} \left[1 - \left(\ln \frac{E_0}{\epsilon} \frac{kT}{\mu(T)b^3g_0}\right)^{2/3}\right]. \quad (4)$$

If the normalization procedure with respect to temperature is correct, then a plot of $(\sigma/\mu(T))^{1/2}$ versus $(kT/\mu(T)b^3)^{2/3}$ for the reload experiments at constant strain rate but varying temperature should yield a straight line. The intercept at zero temperature in this plot gives the mechanical threshold normalized by the shear modulus while the slope is inversely related to the normalized activation energy. The data from the reload experiments are plotted on these coordinates in Fig. 4. Included in Fig. 4 are results obtained previously¹⁰ at a strain of 0.10 and strain rates of 0.0014 s^{-1} , 0.82 s^{-1} and 5000 s^{-1} . These latter data include reload experiments at $\sim 200 \text{ K}$ which gives data at three temperatures and allows an evaluation of the normalization procedure described above as well as of the exponents chosen in Eq. 3. No tests at the intermediate

temperature could be performed on the shock recovered specimens due to the limited number of samples. The values of the mechanical threshold (referenced to 297 K) and the normalized free energy for the shock recovered material are listed in Table 1 along with previously obtained values for lower strain rates. The latter data are grouped into two categories to show comparisons at uniform strain as well as at uniform mechanical threshold.

Table 1. Measured Values of $\hat{\tau}$ and g_0

	$\underline{\epsilon}$	$\underline{\dot{\epsilon}}$	$\underline{\hat{\tau}} (297 \text{ K})$	$\underline{g_0}$
10 GPa Shock	.0825	(10 GPa)	314	$0.80 \times 10^{21} \text{ Nt-m}$
Uniform Strain	.10	.00014 s^{-1}	179 MPa	9.4
	.10	.015	187	5.7
	.10	.82	191	6.0
	.10	81	204	1.9
	.107	1800	218	6.8
	.10	5000	228	3.3
	.087	9500	212	4.8
Uniform Mechanical Threshold	.25	.82	309	2.07
	.25	81	329	1.88
	.209	1800	309	2.08
	.211	5000	325	1.43

In the previous study, mechanical threshold values were obtained as a function of strain. By interpolating these results, we have plotted in Fig. 5 the mechanical threshold values at a single strain of 0.0825, which corresponds to the transient plastic strain during the shock-deformation. The actual strain rate for the 10 GPa shock is unknown and, in fact, probably varies significantly between the loading and unloading portions of the wave. For Fig. 5 the strain rate during the shock is assumed to

lie within the range 10^5 s^{-1} to 10^6 s^{-1} ; the lower limit is set by the transient strain divided by the pulse duration.

Substructure Observations

Optical and TEM micrographs of the 10 GPa shock-deformed copper are shown in Figs. 6 - 8. The micrographs reveal evidence of a highly dislocated structure with a percentage of grains exhibiting fine parallel markings (seen optically in Fig. 6) which TEM and selected-area diffraction (SAD) analysis verify as deformation twins. The predominant deformation substructural feature, that of dislocation cells, is consistent with numerous previous studies on shock-loading of copper^{2,4,12,13} at moderate pressures. Dislocation loops were also observed within some cell interiors.

Depending upon orientation, grains were found to exhibit entirely cellular dislocation, deformation twinned, or a mixed substructural morphology. Additionally a small fraction of grains exhibited bands of high dislocation density⁴ lying on {111} planes; these may be features identified as microbands which have been observed in heavily cold rolled copper¹⁴.

DISCUSSION

The mechanical threshold measurements lead to several interesting conclusions. The comparisons shown in Table 1 and Fig. 5 indicate that at equivalent strain, the mechanical threshold increases dramatically in the shock-deformation regime. In fact, as shown in Fig. 5, the increase begins at strain rates closer to 10^3 s^{-1} . The mechanical threshold is a mechanical measure of structure, and for dislocation hardening alone the mechanical threshold is related to the total dislocation density ρ by¹⁵

$$\hat{\tau} = \mu b \rho^{1/2} . \quad (5)$$

If the sole difference between the quasi-static deformation and shock-deformation were in the rate of dislocation storage, then from Eq. 5 and from the data in Table 1 the dislocation density in a shock-deformed sample should be approximately three times that in a sample quasi-statically deformed to a strain of 0.10. While it is well documented using measurements of resistivity⁵, energy storage⁵, and actual dislocation counts in TEM foils⁴ that the dislocation densities in shock-deformation exceed those in quasi-static deformation, the experimental techniques for measuring the dislocation density are probably not precise enough to verify this factor of three estimate.

The other comparison shown in Table 1 is that of the normalized activation energy at constant threshold stress. The value for the shock-deformed material, $g_0 = 8.0 \times 10^{20} \text{ Nt-m}$, is roughly one-half the values at the lower strain rates. This suggests that the obstacle in the

former is slightly more rate sensitive than that in the latter. Comparison of the values of g_0 at the lower strain rates with those at the higher strain rates in Table 1 shows a general trend toward a decreasing g_0 . However, a factor of two is small and, given that the estimate of g_0 is made from the slope of the fit in Fig. 4, the error in this estimate may be large. For comparison, mechanical threshold measurements on a solid solution hardened austenitic stainless steel¹⁰ yielded a normalized activation energy equal to 0.5×10^{20} Nt-m, which suggests that the small difference noted in Table 1 between the shock hardened material and material strained at lower strain rates is probably not significant.

Microscopic characterization of the shock-deformed microstructure tends to support the conclusions based on the mechanical threshold measurements. The observed structure was heavily dislocated and contained well developed cellular structures. At a shock pressure of 10 GPa, a few grains deform solely by deformation twinning while in other grains both twins and cellular dislocation structures are observed. It is unclear what influence the twins have on the mechanical threshold measurements. Since the increase in the dependence of the mechanical threshold on strain rate begins at strain rates as low as 10^3 s^{-1} , where deformation twinning definitely has not been found, the observed twinning at 10 GPa probably has not influenced the mechanical threshold measurements.

Although some observations of the shock-deformed microstructure are consistent with higher levels of vacancy production, this does not appear to be a dominant feature. The mechanical threshold measurements also show

no evidence of a dramatically increased density of a second, more rate sensitive, defect, which vacancy loops or clusters might be expected to provide.

The conclusion based on the experiments described here is that the mechanical threshold measurements are consistent with measurements obtained at lower strain rates. The mechanical threshold of shock-deformed copper exceeds that of quasi-statically and even dynamically ($\dot{\epsilon} = 10^4 \text{ s}^{-1}$) deformed copper. It appears as if the high strain rates achieved during the shock process lead to increased levels of dislocation storage, which are consistent with trends noted at strain rates exceeding 10^3 s^{-1} .

Measurements of the mechanical threshold provide another tool with which to study shock-deformation mechanisms. These experiments should be extended to other materials and to the investigation of effects of peak pressure, pulse duration and rarefaction rate on the structure evolution during shock-deformation.

ACKNOWLEDGEMENTS

The authors wish to acknowledge C. Frantz and B. Jacquez for their assistance in the design and performance of the shock-loading experiment, M. Lopez for his capable optical metallography skills, and P. Martin for assisting with the interpretation of the TEM study. This work was performed under the auspices of the U. S. Department of Energy with

support from the Los Alamos National Laboratory Center for Materials Science.

REFERENCES

1. W. C. Leslie, Microstructural effects of high strain rate deformation, in: "Metallurgical Effects at High Strain Rates," R. W. Rohde, B. M. Butcher, J. R. Holland, and C. H. Karnes, eds., Plenum Press, New York (1973).
2. L. E. Murr, Residual microstructure-mechanical property relationships in shock-loaded metals and alloys, in: "Shock Waves and High-Strain-Rate Phenomena in Metals," M. A. Meyers and L. E. Murr, eds., Plenum Press, New York (1981).
3. D. E. Mikkola and R. N. Wright, Metallurgical effects of shock loading, in: "Shock Waves in Condensed Matter-1981," W. J. Nellis, L. Seaman, and R. A. Graham, eds., American Institute of Physics, New York (1982).
4. J. George, An electron microscope investigation of explosively loaded copper, Phil. Mag. 15:497 (1967).
5. D. C. Brillhart, R. J. De Angelis, A. G. Preban, J. B. Cohen and P. Gordon, Quantitative study of the substructure and properties of shock-loaded copper, AIME Trans. 239:836 (1967).
6. H. Kressel and N. Brown, Lattice defects in shock-deformed and cold-worked nickel, J. Appl. Phys. 38:1618 (1967).
7. R. A. Graham, Active measurements of defect processes in shock-compressed metals and other solids, in: "Shock Waves and High-Strain-Rate Phenomena in Metals," M. A. Meyers and L. E. Murr, eds., Plenum Press, New York (1981).
8. U. F. Kocks, A. S. Argon and M. F. Ashby, "Thermodynamics and Kinetics of Slip," Prog. Mtl. Sci. 19, Pergamon Press, New York (1975).
9. P. S. Follansbee, G. Regazzoni and U. F. Kocks, The transition to drag-controlled deformation in copper at high strain rates, in: "Mechanical Properties at High Rates of Strain," Inst. Phys. Conf. Ser. No. 70, J. Harding, ed., Institute of Physics, London (1984).
10. P. S. Follansbee, U. F. Kocks and G. Regazzoni, The mechanical threshold of dynamically deformed copper and Nitronic 40, to be published in: "Proceedings of the International Conference on Mechanical and Physical Behavior of Material under Dynamic Loading," Paris, France (1985).
11. A. S. Appleton and J. S. Waddington, Some observations of discontinuous yielding phenomena in copper, nickel and aluminum after shock loading, Phil. Mag. 12:273 (1965).
12. A. S. Appleton and J. S. Waddington, The importance of shock wave profile in explosive loading experiments, Acta Met. 12:956 (1964).
13. O. Johari and G. Thomas, Substructures in explosively deformed Cu and Cu-Al alloys, Acta Met. 12:1153 (1964).
14. A. S. Mallin and M. Hatherly, Microstructures of cold-rolled copper, Metal Sci. ??:463 (1973).

15. H. Mecking and J. F. Kocks, Kinetics of flow and strain hardening, Acta Met. 29:1865 (1981).

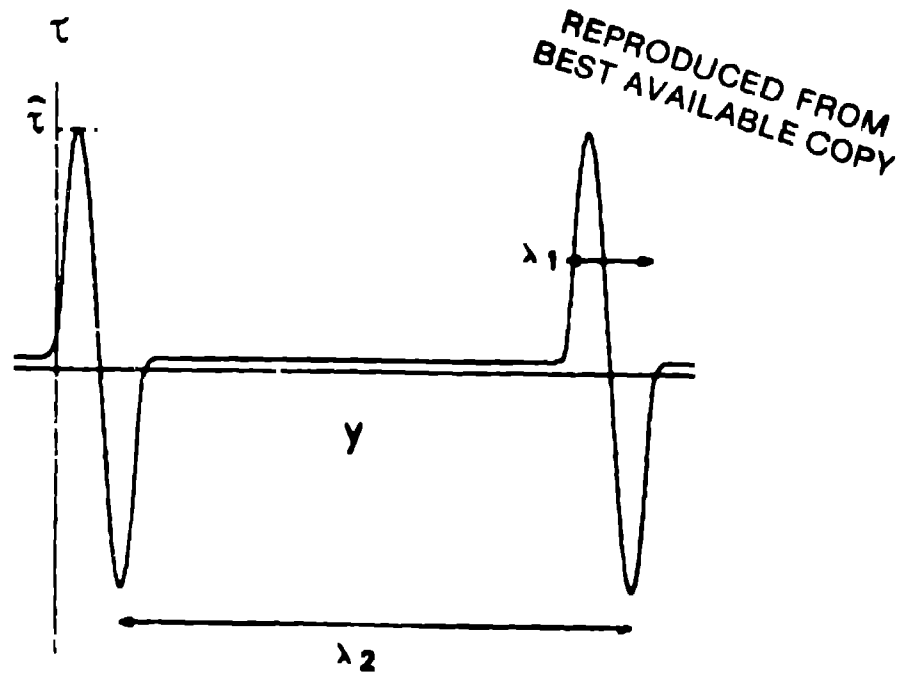


Figure 1: Glide resistance profile showing the interaction between a mobile dislocation and two short range ($\lambda, \ll \lambda_2$) obstacles separated by a distance λ_2 .

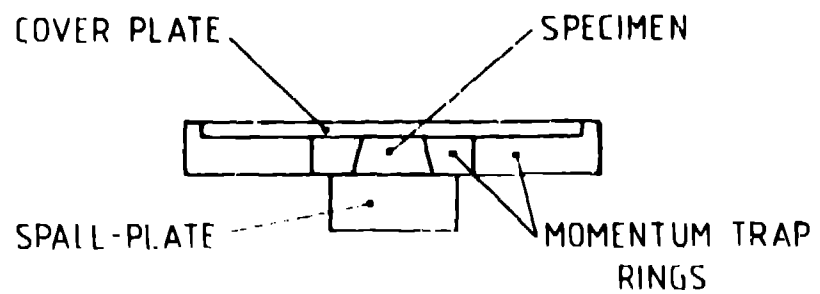
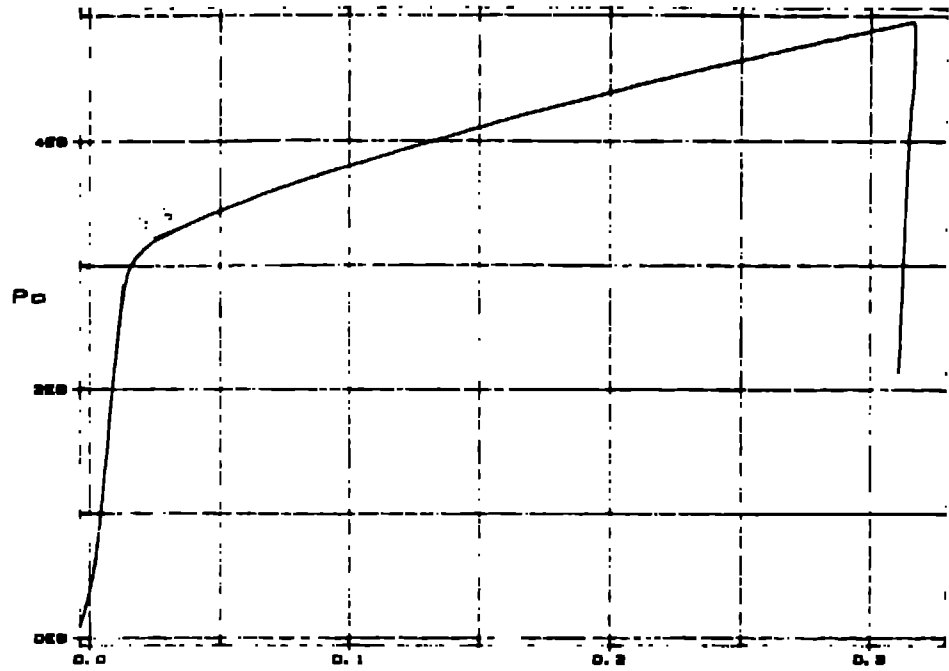


Figure 2: Schematic of shock-loading specimen assembly

10 GPA CU TEST 11 - 76K RELOAD #1 TRUE

REPRODUCED FROM
BEST AVAILABLE COPY



10 GPA CU TEST 11 - RT RELOAD #3 TRUE

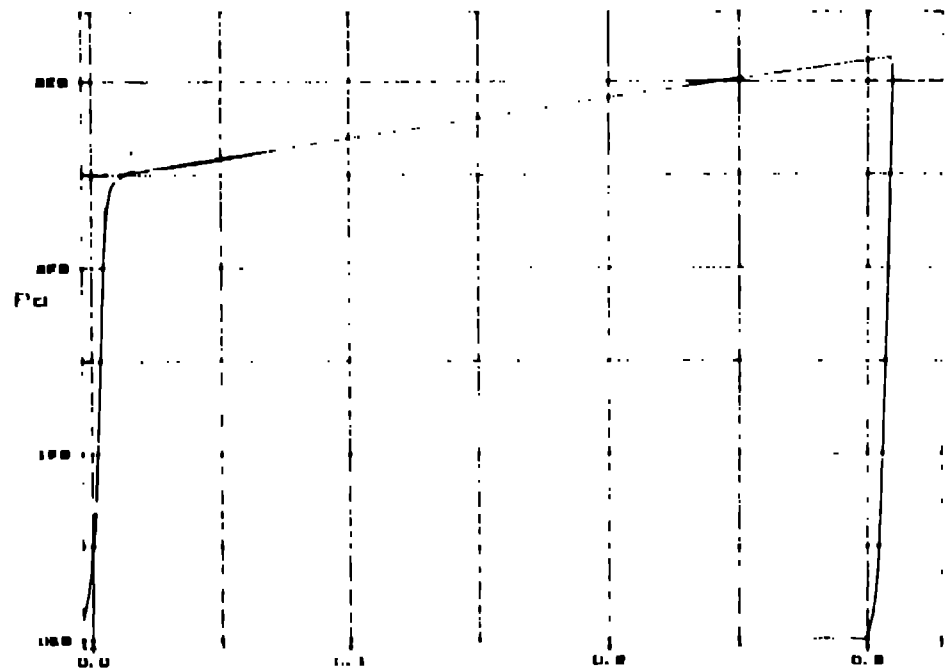


Figure 3: Stress strain curves for quasi-static reloading at 297 K and 76 K following 10 GPa shock deformation.

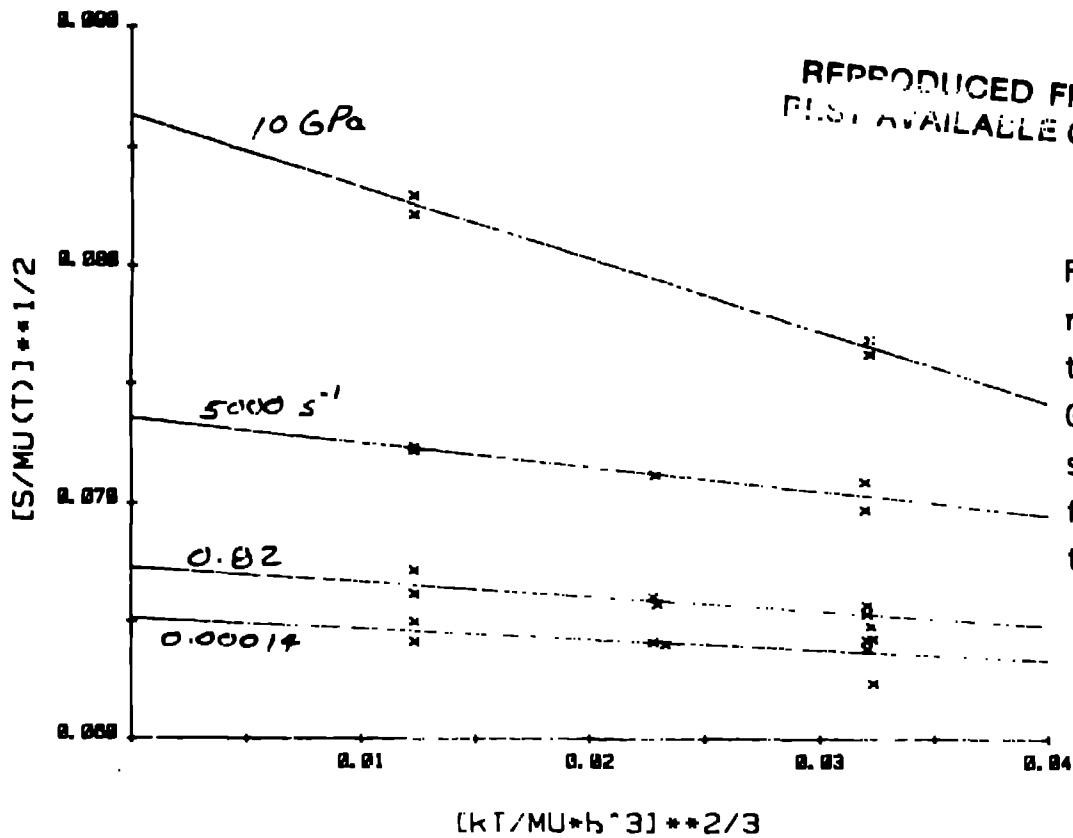


Figure 4: Normalized plot of reload yield stress versus test temperature for the 10 GPa shock-deformed copper sample and three samples deformed at lower strain rates to a strain of 0.10

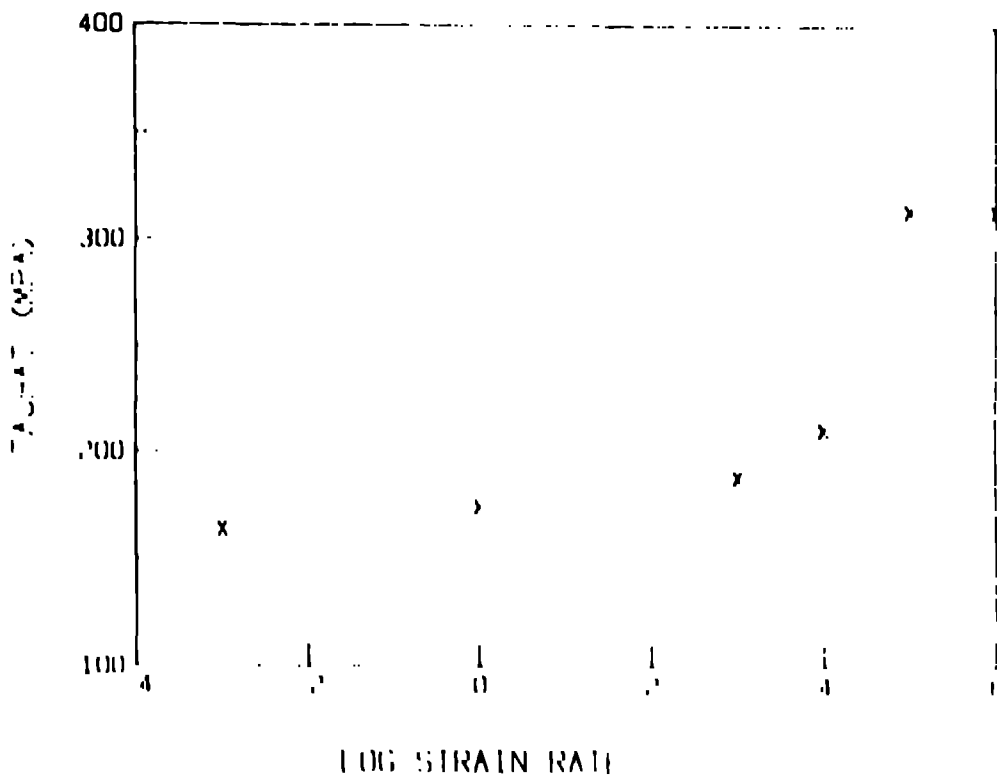


Figure 5: Variation of the mechanical threshold at a uniform strain of 0.0825 with strain rate.

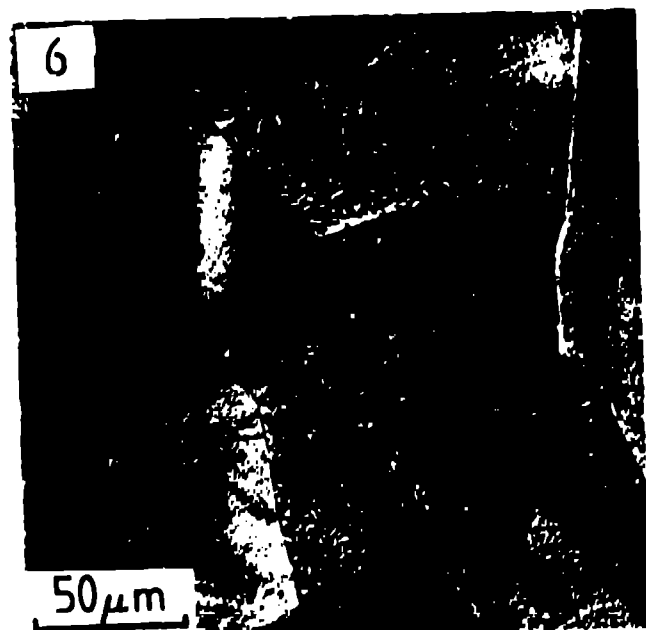


Figure 6: Optical micrograph of shock-deformed copper showing twinned and heavily dislocated (etch pits) structure.

Figure 7: Bright field electron micrograph of cellular dislocation substructure in shock-loaded copper $\langle 213 \rangle$ zone.

Figure 8a: Bright field electron micrograph of deformation twin substructure in shock-deformed copper.

Figure 8b: Selected area electron diffraction pattern of Fig. 8a illustrating twin reflections in $\langle 110 \rangle$ zone.